




Optimizing magnetically shielded solenoids

Cite as: Rev. Sci. Instrum. **91**, 105102 (2020); <https://doi.org/10.1063/5.0022547>

Submitted: 21 July 2020 . Accepted: 15 September 2020 . Published Online: 02 October 2020

W. C. Chen , Md. T. Hassan , R. Erwin, S. M. Watson, T. R. Gentile, and G. L. Jones 





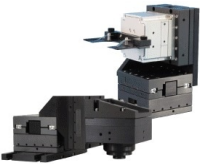
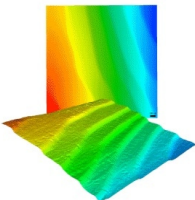
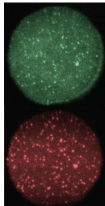
View Online



Export Citation



CrossMark

 MCL MAD CITY LABS INC. www.madcitylabs.com	<p>Nanopositioning Systems</p> 	<p>Modular Motion Control</p> 	<p>AFM and NSOM Instruments</p> 	<p>Single Molecule Microscopes</p> 
---	--	--	---	--

Optimizing magnetically shielded solenoids

Cite as: Rev. Sci. Instrum. 91, 105102 (2020); doi: 10.1063/5.0022547

Submitted: 21 July 2020 • Accepted: 15 September 2020 •

Published Online: 2 October 2020



W. C. Chen,^{1,a)} Md. T. Hassan,^{1,2} R. Erwin,¹ S. M. Watson,¹ T. R. Gentile,¹ and G. L. Jones³

AFFILIATIONS

¹NIST Center for Neutron Research, National Institute of Standards and Technology, Gaithersburg, Maryland 20899, USA

²Department of Materials Science and Engineering, University of Maryland, College Park, Maryland 20742, USA

³Department of Physics, Hamilton College, Clinton, New York 13323, USA

^{a)}Author to whom correspondence should be addressed: wcchen@nist.gov

ABSTRACT

An important consideration when designing a magnetostatic cavity for various applications is to maximize the ratio of the volume of field homogeneity to the overall size of the cavity. We report a design of a magnetically shielded solenoid that significantly improves the transverse field gradient averaged over a volume of 1000 cm³ by placing compensation coils around the holes in the mu-metal end caps rather than the conventional design in which the compensation coils are placed on the main solenoid. Our application is polarized ³He-based neutron spin filters, and our goal was to minimize the volume-averaged transverse field gradient, thereby the gradient induced relaxation time, over a ³He cell. For solenoids with end cap holes of different sizes, additional improvements in the field gradient were accomplished by introducing non-identical compensation coils centered around the non-identical holes in the end caps. The improved designs have yielded an overall factor of 7 decrease in the gradient in the solenoid, hence a factor of 50 increase in the gradient induced relaxation time of the ³He polarization. The results from both simulation and experiments for the development of several such solenoids are presented. Whereas our focus is on the development of magnetically shielded solenoids for ³He neutron spin filters, the approach can be applied for other applications demanding a high level of field homogeneity over a large volume.

<https://doi.org/10.1063/5.0022547>

I. INTRODUCTION

In the last two decades, polarized ³He gas has attracted considerable interest in a wide range of applications including neutron spin filters (NSFs),^{1–5} spin-polarized targets,^{6,7} and magnetic resonance imaging.⁸ An overview of the full range of applications can be found in a recent review article.⁹ Our focus is on neutron spin filters, which rely on the large spin dependence of the cross section for absorption of neutrons by ³He gas and are employed at several neutron facilities for spin-polarizing and spin-analyzing slow neutron beams. A polarized neutron experiment is often limited by the relatively low fluence of polarized neutron beams, so it is necessary to maximize the time-averaged neutron polarization and transmission for a polarized neutron experiment using ³He NSFs. This presents the need to maximize the time-averaged ³He polarization for a given experiment. Two possible approaches have been developed to accomplish this goal. First, a continuously operating ³He NSF system based on the spin-exchange optical pumping (SEOP) method was developed to maintain a constant ³He polarization.¹⁰ This system, named *in situ* SEOP, typically takes up significant space,

which may not be available on a neutron beamline, particularly when a ³He NSF is retrofitted to an existing instrument. In addition, high power lasers must be located on the beamline. When *in situ* SEOP operation is not feasible due to a space constraint on the instrument, a more compact, remotely operating ³He NSF system using ³He gas polarized from either a SEOP or metastability-exchange optical pumping (MEOP) system in the lab has been used.^{1,2} In this scheme, it is necessary to maintain the ³He polarization relaxation time on a neutron beamline as long as possible, typically from a hundred hours to several hundred hours.

The relaxation time T_1 of the polarized ³He gas has three contributions, (1) dipole–dipole interactions,¹¹ T_1^{dd} ; (2) wall relaxation,¹² T_1^{w} ; (3) magnetic field gradients,¹³ T_1^{fg} , and is given by

$$\frac{1}{T_1} = \frac{1}{T_1^{\text{dd}}} + \frac{1}{T_1^{\text{w}}} + \frac{1}{T_1^{\text{fg}}} = \frac{1}{T_1^{\text{i}}} + \frac{1}{T_1^{\text{fg}}}, \quad (1)$$

where T_1^{i} is the intrinsic relaxation time and characteristic of each cell. The dipole–dipole relaxation rate increases linearly with the

partial pressure p of ^3He gas and is given by $1/T_1^{\text{dd}} = p/807 \text{ (h}^{-1}\text{)}$ for p in bar.¹¹ For ^3He NSF applications, the ^3He pressure typically ranges from 1 bar to 2 bars, corresponding to T_1^{dd} of $\approx 800 \text{ h}$ and $\approx 400 \text{ h}$, respectively. In the case of thermal or hot neutrons, the pressure can be as high as 3 bars, corresponding to T_1^{dd} as short as $\approx 270 \text{ h}$. The current best ^3He cell fabrication practice has nearly eliminated the wall relaxation rate ($1/T_1^{\text{w}} < 1/3000 \text{ h}^{-1}$) in certain ^3He cells.^{14,15} The field gradient is typically the dominant limitation to the overall relaxation time for a NSF application. To make a magnetostatic device more practically feasible, a field gradient induced relaxation time T_1^{fg} of 600 h or longer is desired at a modest ^3He pressure between 1 bar and 2 bars so that the overall relaxation time T_1 would be better than between 344 h and 241 h for a cell with negligible wall relaxation.

The magnetic field gradient induced relaxation is a spin-lattice relaxation of the ^3He nuclei due to the magnetic field fluctuations from the Brownian motion of the spins in the presence of a magnetic field gradient.¹³ The relaxation rate $1/T_1^{\text{fg}}$ due to magnetic field gradients is directly proportional to the square of the fractional transverse field gradients and inversely proportional to the ^3He pressure.¹³ At room temperature, $1/T_1^{\text{fg}}$ is given by¹⁶

$$\begin{aligned} \frac{1}{T_1^{\text{fg}}} &= \frac{6700}{pV} \int \int \int_V \left(\frac{|\vec{\nabla} B_x|^2}{B^2} + \frac{|\vec{\nabla} B_y|^2}{B^2} \right) dx dy dz \text{ h}^{-1} \\ &\equiv \frac{6700}{p} |\vec{\nabla} B_{\perp}/B|^2 \text{ h}^{-1}, \end{aligned} \quad (2)$$

where $\frac{\vec{\nabla} B_x}{B}$ and $\frac{\vec{\nabla} B_y}{B}$ are the gradients in the transverse components of the magnetic field using the coordinate system in Fig. 1 (for nuclear polarization along the z axis) normalized to the central field, B , in units of cm^{-1} . $|\vec{\nabla} B_{\perp}/B|$ is the normalized volume-averaged transverse gradient (NVATG) over the cell volume V and is $\approx 5 \times 10^{-4} \text{ cm}^{-1}$ for $T_1^{\text{fg}} = 600 \text{ h}$. However, these transverse components are too tiny ($< 1 \mu\text{T}$) to be measured accurately for a field gradient level of 10^{-4} cm^{-1} using conventional means. What has been typically done to optimize the field gradient when characterizing a magnetostatic cavity device is to measure the conveniently

measurable gradient component along the applied field. In prior development of magnetostatic cavity devices, we demonstrated that the conveniently measurable normalized line-averaged gradient (NLAG) could be used to be a good indicator of the NVATG of an end-compensated magic box.¹⁷ In this paper, we demonstrate and employ the same approach for the characterization and optimization of magnetic shielded solenoids (MSSs).

For neutron spin filter applications, polarized ^3He gas is typically maintained in a spatially homogeneous magnetic field provided by either a MSS or a magic box¹⁸ on a neutron beamline. In an unshielded solenoid with a finite length or aspect ratio, compensation coils on the main solenoid at the ends or correction coils at different locations have been employed to improve the field homogeneity.¹⁹ Correction coils in an unshielded solenoid have typically been used to obtain a high level of field homogeneity for high precision measurements. A magnetic shielded solenoid consists of a solenoid enclosed in a cylindrical mu-metal shield concentric to the solenoid with or without a cap on each end of the shield. The mu-metal shield reduces the effects of external stray magnetic fields and improves the field homogeneity of a solenoid.¹⁹ Several developments of MSSs have been reported. The first version of the MSS development by Hanson and Pipkin reported a design of three layers of magnetic shielding for a MSS of 33 cm diameter and 92 cm length for atomic physics applications.¹⁹ In their design, the authors did not use compensation coils; instead, they used a series of correction coils arranged at several appropriate locations to cancel the first order and higher order terms in the field profile of a solenoid. They demonstrated a line-averaged field gradient along the applied field of better than $1 \times 10^{-4} \text{ cm}^{-1}$ over an 8 cm diameter sphere. However, the device is too large to be practically fit on most neutron beamlines, and the hole size of 7.6 cm in diameter on the end cap for the beam path of light¹⁹ is not large enough for many NSF applications.

NSF applications are typically constrained by space along the beamline but are able to tolerate larger field gradients on the order of $5 \times 10^{-4} \text{ cm}^{-1}$ so that a MSS can be designed to be more compact. Beam holes on each of the end caps are often desired for a ^3He NSF for a modern neutron scattering instrument. In recent development of a MSS, a conventional approach in which the compensation coils are located on the main solenoid at ends was employed.^{10,20–23} The resulting field gradients are reasonably small and acceptable for certain applications. However, the device either occupied a large amount of space or was employed for a small neutron beam so that the ratio of the volume of the homogeneous field region to the occupied volume of the device is not optimized. This is important when a MSS is designed to retrofit to an existing instrument where the space for implementation of a MSS is limited. Kira *et al.* reported a design of MSS with compensation coils on the main coil and two side coils placed at the windows of the neutron beam to suppress the depolarization of the polarized neutron beam.²⁴ This work is to present a different approach to significantly improve field gradients of short solenoids compared to the conventional configuration. Field homogeneity was improved by placing the compensation coils only around the holes of mu-metal end caps. In addition, we introduce the concept of non-identical compensation coils together with non-identical holes on each of the end caps that are used to match focusing or divergence of an incident or scattered neutron beam, respectively. We show in this paper that the non-identical compensation coil configuration can further decrease the field gradient.

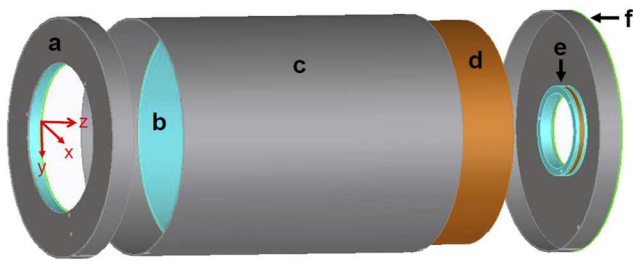


FIG. 1. Schematic of a MSS with round holes on the end caps. The neutron beam travels from right to left in this design. The MSS has the following components: (a) Co-NETIC²⁸ mu-metal end caps, (b) the aluminum solenoid with a wall thickness of 2.4 mm for support of the copper winding, (c) Co-NETIC mu-metal cylinder, (d) copper winding, (e) compensation coils either attached to the end cap (design in this work) or wound on the main coil, and (f) borated aluminum neutron shielding pieces attached to the upstream end cap and the downstream compensation coil (not visible).

Development of MSSs for improving the relaxation times of the ^3He NSFs on the neutron beams at the National Institute of Standards and Technology (NIST) Center for Neutron Research (NCNR) began for a thermal triple axis spectrometer (TAS) more than 10 years ago²⁵ and has continued for a wide variety of instruments since then.^{2,26,27} However, the instrumentation was the main focus in those previous publications, and no systematic studies on the design and optimization of the MSSs were reported. This paper provides extensive details of the development of MSSs motivated for several specific applications over the past decade. Simulation and optimization for parametric studies were done only for those MSSs targeted for specific applications. However, the method presented here should be applicable for the design of any MSS.

II. DESIGN

In order to fit a MSS on a beamline at the NCNR, we typically determined the dimensions of each component with the aim of designing the solenoid as compact as possible but achieving the NVATG better than $5 \times 10^{-4} \text{ cm}^{-1}$. Space constraints originate not only from the neutron instrument itself but also from the need for adiabatic spin rotation devices to manipulate the neutron spin and/or a radio-frequency (RF) coil within the solenoid to flip the ^3He spin using the adiabatic fast passage (AFP) nuclear magnetic resonance (NMR) method. The most important criteria are to determine the diameters of the hole of each of the end caps and the aspect ratio that is defined to be the ratio of the length to the diameter of the main solenoid. The diameters of the hole of end caps are directly related to the diameter of a ^3He cell. It is always desired for a MSS and the ^3He cell to provide a full coverage of the required beam size regardless of whether the ^3He cell is used as a polarizer or an analyzer.

Figure 1 shows a schematic of a typical MSS with circular holes on each of the end caps. A single layer of 16 AWG (American Wire Gauge) copper wire (7.30 turns/cm) was wound on an aluminum cylinder that is nested inside a mu-metal cylinder. The gap between the outer diameter of the solenoid and the inner diameter of the mu-metal shield is typically chosen from 7 mm to 9 mm to protect the mu-metal from saturation and minimize the field gradient, given a fixed configuration of the aluminum solenoid. On each end of the mu-metal shield, a mu-metal end cap is attached to the mu-metal cylinder body with an overlap of 2.5 cm. The overlap forms a magnetic connection between the end cap and the body and protects the mu-metal from saturation even when applying a modest current to the aluminum solenoid. Perfection annealed Co-NETIC²⁸ mu-metal has been used for both the mu-metal cylinder and end caps. The thickness for the mu-metal pieces is 1.6 mm. A compensation coil is attached and centered around the hole in each end cap. The end caps were designed to be snugly fitted onto the mu-metal cylinder body to allow for convenient and quick ^3He cell exchange (on the order of several seconds) from a MSS to another device maintaining the ^3He polarization or vice versa to minimize the loss of the ^3He polarization during the transfer. It has been determined that this loss is negligible in our setup. There is a circular hole on each end cap to let neutrons pass through without neutron depolarization. Other features in Fig. 1 include borated aluminum neutron shields attached to both the upstream end cap and the downstream

compensation coil frame. The borated aluminum structures serve as neutron shielding. Not shown in Fig. 1 is an RF coil that is used to invert the ^3He polarization. The RF coil is an important consideration of space when designing a MSS, but is not a topic here.

As discussed later, a further improvement in the field gradient can be made by employing non-identical compensation coils on the end caps. Practically, this implies that a MSS can be made even more compact without losing the angular coverage for a focusing or divergent neutron beam. An additional benefit using non-symmetric compensation coils is a possibility of reducing the diameter of the ^3He cell for the same angular coverage since the most homogeneous part of the field is shifted toward the sample, which is presumably at the focal point of the beam. This means that the center with the same field homogeneity is always closer to the smaller end cap hole than the larger one, which is the downstream end cap for the polarizer and the upstream end cap for the analyzer.

III. SIMULATION

The finite-element software package RADIA²⁹ was employed to calculate the field, and the Mathematica³⁰ interface was used for analytical calculation of the magnetic field gradients. The B-H data for Co-NETIC mu-metal was provided by the manufacturer, with a saturated B reduced from 0.78 T to 0.69 T, as discussed in Ref. 17. The criterion for convergence of the RADIA simulation iterations was that the magnetization of all segments changed by less than 10 nT. The segment size was set to be $\approx 4.6 \text{ mm}$ along z and 6.67° radially in the xy plane below which point the NVATG changed by less than 10^{-5} cm^{-1} .

We focused on two configurations of compensation coils with the overall goal to improve the field gradients. The first one represents the compensation coils of the same diameter centered around the hole of each of the end caps and is denoted as *identical hole compensation*. This is compared with a conventional design in which the identical compensation coils are placed on the main solenoid at the ends,^{10,20–23} denoted as *end compensation*. Figure 2 shows a schematic of such configurations of compensation coils for comparison. A cylindrical ^3He cell with a diameter slightly larger than that of the end cap hole is also shown for the purpose of calculating the NVATG. The second configuration includes holes of different sizes on the two ends of the shield, which are matched to the divergence of the neutron beam. In the second case, the compensation coils are matched to the holes in the end caps and are therefore also different from each other. This configuration is denoted as *non-identical hole compensation*. This design represents a further improvement in the NVATG as compared to the first one, given the same space constraint. Figure 3 shows a schematic drawing of both the identical and non-identical hole compensation configurations.

We began by computing the NVATGs and NLAGs $|\partial B_z / \partial z|/B$ so as to show that optimization of the NLAG is a signature of optimization of the NVATG. We followed the same procedure as developed for a magic box.¹⁷ To optimize a MSS, both a NVATG and a NLAG are computed by varying the number of turns of the compensation coil after a field contour map is generated. We show the calculation for identical and non-identical hole compensation. The six transverse field gradients are integrated over a cylindrical cell

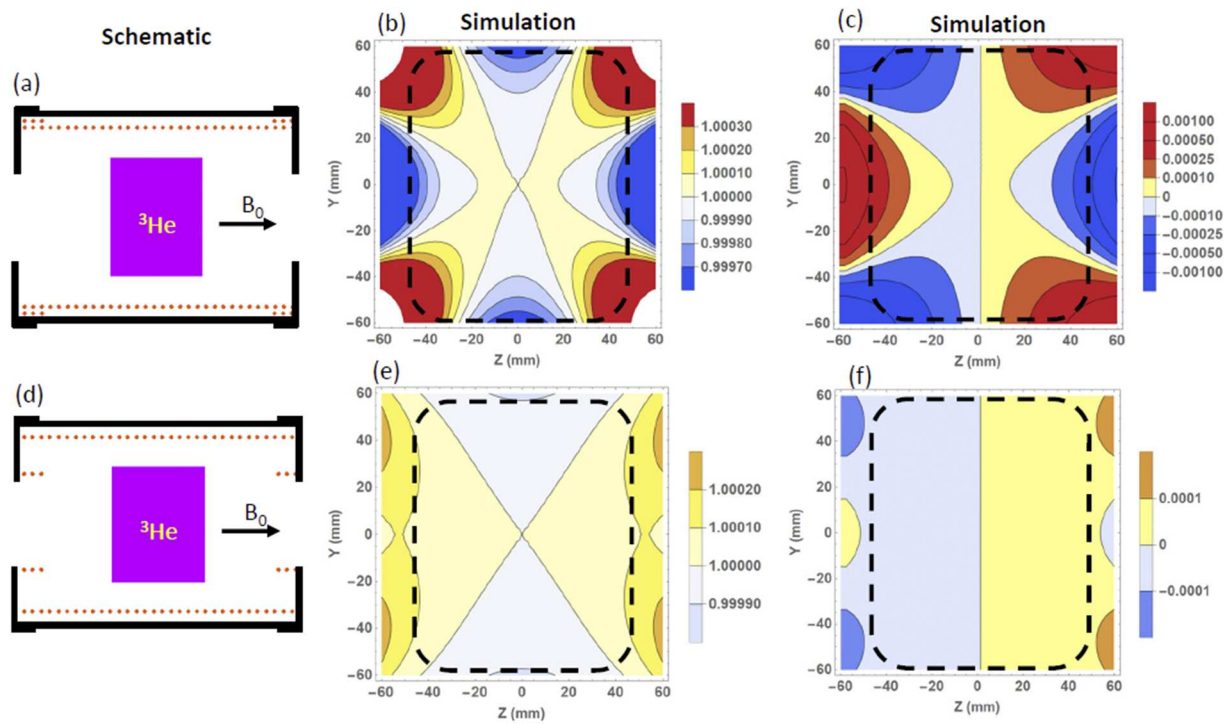


FIG. 2. Schematic [(a) and (d)] of end compensation and identical hole compensation configurations in a MSS and corresponding contour plots of the calculated normalized B_z profile [(b) and (e)] and the calculated $|\partial B_z/\partial z|/B$ profile [(c) and (f)] in the central plane ($x = 0$) for the region in which the ^3He cell is contained. $|\partial B_z/\partial z|/B$ is in cm^{-1} . (a)–(c) refer to the conventional end compensation approach. (d)–(f) refer to the identical hole compensation approach. The mu-metal body and end cap are shown in black. Long dotted lines close to the mu-metal cylinder body represent the winding of the main solenoid, while the short ones represent the winding of the compensation coils. The black dashed line box indicates a region in which the volume-averaged field gradient is the smallest and a ^3He cell should be positioned. Note that the contour intervals between (b) and (e) and between (c) and (f) are the same, but the ranges are different for the two schemes due to a significant difference in the gradient.

volume of 12 cm in diameter and 10 cm long. The cylindrical ^3He cell is co-axial with the MSS. The NLAG is integrated over 10 cm along the applied field direction (z). Both integrations were done within the most homogeneous region of the field. The results are plotted in Fig. 4 for the MSS Gemini³¹ with the end compensation and for the MSS Honesty with non-identical hole compensation. The field strengths in the solenoids were set to correspond to the NMR frequencies at which the AFP flipping was optimized; hence, these values (2.73 mT for Gemini and 2.85 mT for Honesty) were employed for the simulation. For the calculation of the non-identical hole compensation configuration, two curves were calculated, one with the number of turns of the compensation coil fixed for a smaller end cap hole and the other with the number of turns of the compensation coil fixed for a larger end cap hole, since a significant difference in the number of turns of the compensation coil at optimization is expected due to the asymmetry along the z direction. Figure 4(b) shows the result when the number of turns of the compensation coil was fixed at the larger end cap hole. It can be seen that not only does the NLAG minimize at the same location as the NVATG, but also it is much more sensitive to the change in the number of compensation turns. This demonstrates that the NLAG can indeed be used as a direct evaluation criterion for minimizing the NVATG when experimentally optimizing a MSS.

Having established the relationship between the volume- and line-averaged gradients, we have modeled four different MSSs with different dimensions for different polarized neutron instrument applications at the NCNR. For each MSS, we simulated the 3D magnetic field profiles of B_x , B_y , and B_z . Although the transverse components B_x and B_y are important for the calculation of the gradients, they are small and not what were experimentally measured. Only the contour plots of the experimentally measurable field B_z are presented here.

Two configurations of the compensation coil, as shown in Fig. 2, were first modeled using the MSS Gemini mainly because Gemini has identical compensation coils, which is more straightforward to be modeled, and allows for a direct comparison between the two different compensation configurations. The MSS Gemini is 25.4 cm in diameter and 35 cm long and has an end-cap hole diameter of 11.4 cm. For the conventional end compensation configuration, the number of turns of compensation coils was found to be 8 at optimization by seeking the minimum NVATG when varying the number of turns of the compensation coil. The same procedure was followed for the identical hole compensation configuration. The number of turns of compensation coils was then found to be 14 at optimization. For both simulations, the field in the center of the solenoid was fixed at ≈ 2.73 mT. The NVATG $|\vec{\nabla} B_L/B|$

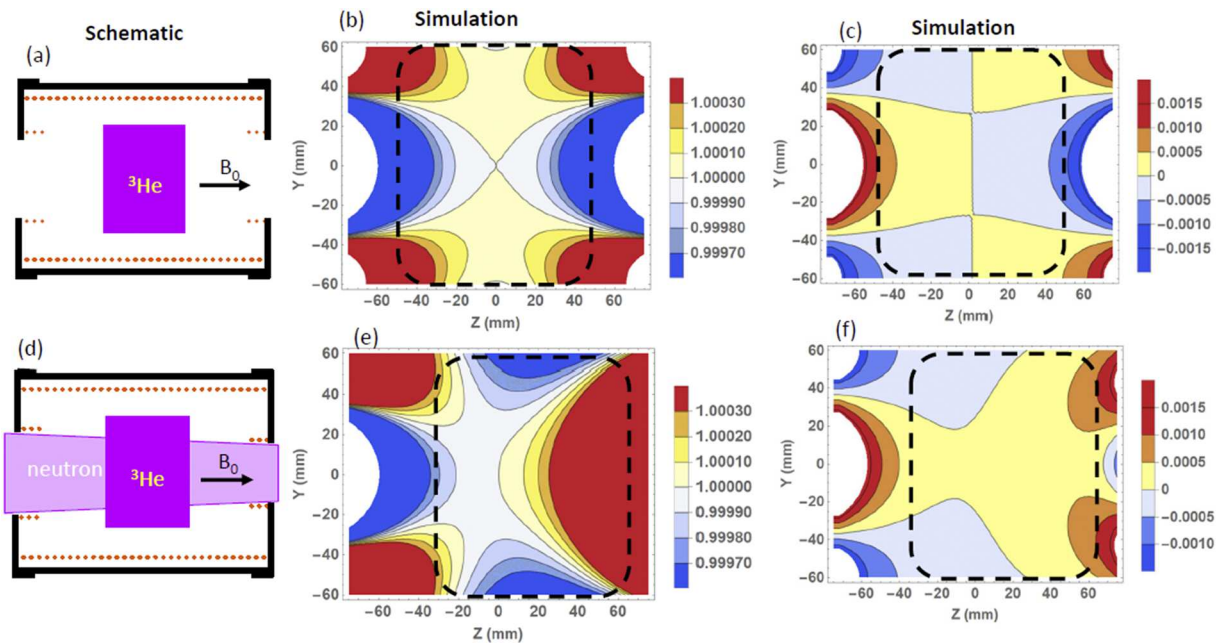


FIG. 3. Schematic [(a) and (d)] of identical and non-identical hole compensation configurations and the corresponding contour plots of the calculated normalized B_z profile [(b) and (e)] and the calculated $|\partial B_z / \partial z| / B$ profile [(c) and (f)] in the central plane ($x = 0$) for the MSS Nyx. $|\partial B_z / \partial z| / B$ is in cm^{-1} . (a)–(c) refer to the identical hole compensation approach. (d)–(f) refer to the non-identical hole compensation approach. The mu-metal body and end cap are shown in black. Long dotted lines close to the mu-metal cylinder body represent the winding of the main solenoid, while the short ones represent the winding of the compensation coils. A focusing neutron beam is drawn to show that the asymmetric hole sizes match the focusing condition. The black dashed line box indicates a region in which the volume-averaged field gradient is the smallest and a ^3He cell should be positioned.

over a cylindrical cell volume of 12 cm in diameter and 10 cm long was determined to be $9.8 \times 10^{-4} \text{ cm}^{-1}$ and $1.2 \times 10^{-4} \text{ cm}^{-1}$ for the conventional end compensation and for the identical hole compensation, respectively. This indicated an improvement

in the NVATG by a factor of 8.2 for the identical hole compensation compared to the end compensation. The corresponding improvement in the field-gradient induced relaxation time T_1^{fg} is a factor of 66. More simulations by changing the location of the

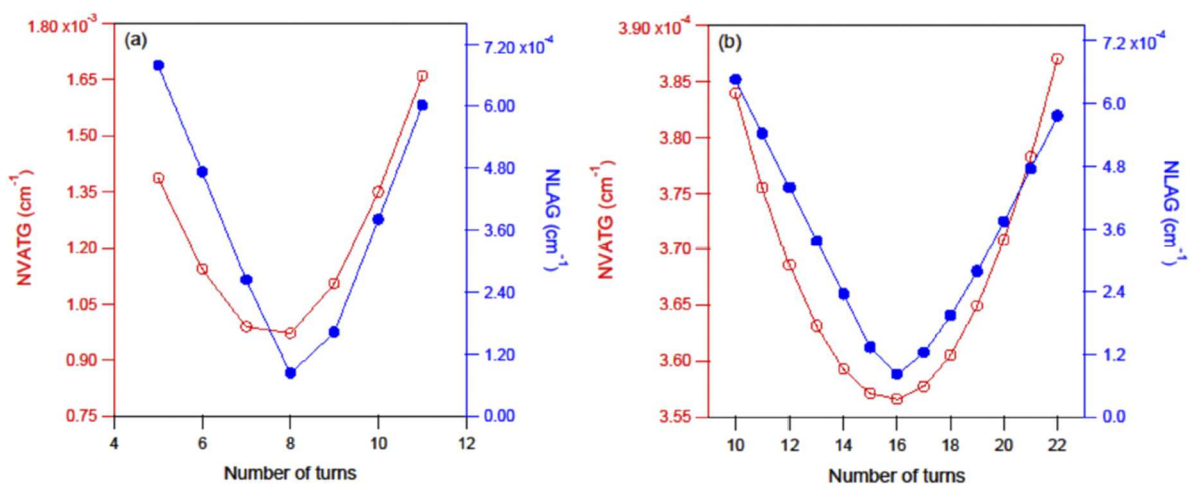


FIG. 4. Calculated NVATGs (red open circles) and NLAGs (blue solid circles) for a 12 cm diameter, 10 cm long cylindrical cell, as a function of the number of turns of the compensation coil for (a) Gemini with the end compensation and (b) Honesty with the non-identical hole compensation. The solid lines are to guide the eye.

compensation coils by varying their diameter while keeping the axial position were done to further demonstrate the significant improvement in the field gradient by compensating the hole of each of the end caps, and the result is shown in Fig. 5. The lowest gradient corresponds to the identical hole compensation configuration. The highest gradient corresponds to the conventional end compensation configuration. Figure 5 clearly demonstrates how the location of the compensation coils improves the field gradient, and hence, compensating the hole yields the lowest gradient.

To visually observe the significant improvement, contour plots of the normalized B_z in the central plane ($x = 0$) of the MSS Gemini for both end and identical hole compensation configurations after optimizing the compensation coil conditions are shown in Fig. 2. It is visually obvious in Fig. 2 that B_z and $|\partial B_z / \partial z|/B$ are substantially more homogeneous in the central plane for the scheme in which the compensation coils are centered around the hole of each of the end caps than that for the conventional scheme.

To further improve the field homogeneity of a MSS, we continued to perform simulation for the non-identical hole compensation configuration. The optimization procedure for such a complicated configuration is different from that for the identical compensation coil configuration since the symmetry along z is broken. A typical procedure for minimizing the field gradient for a MSS with non-identical compensation coils includes the following steps: (1) optimizing a MSS with two sets of identical compensation coils separately, one for the smaller diameter and the other for the larger diameter; (2) varying the number of turns of the smaller compensation coil while fixing the number of turns for the larger compensation coil at optimization determined from step 1; (3) varying the number of turns of the larger compensation coil while fixing the number of turns for the smaller compensation coil at optimization determined from step 2; (3) calculating the NVATG and repeating the above procedure, if necessary, until

the calculated NVATG is minimized and changed by less than 10^{-5} cm^{-1} .

To preserve the angular coverage from a MSS, the identical hole compensation configuration with the larger diameter was used for comparison with the non-identical hole compensation configuration. Figure 3 shows contour plots of the calculated normalized B_z in the central plane ($x = 0$) for the MSS Nyx in both identical hole compensation and non-identical hole compensation configurations. Nyx was developed as a polarizer for BT-7 TAS at the NCTR. Nyx is 25.1 cm in diameter and 29.5 cm long. A compensation hole diameter of 12.6 cm for the identical hole compensation configuration and diameters of 10.3 cm and 12.6 cm for the non-identical hole compensation configuration were used in simulation. It is worthwhile to mention two distinct features: (1) the center of the homogeneous region of the field is shifted $\approx 20 \text{ mm}$ along z closer to the smaller compensation coil for the non-identical hole compensation configuration, while the center is expected at $z = 0$ for the solenoid with the identical hole compensation, and (2) the field is more homogeneous for the non-identical hole compensation configuration, though it is not visually obvious in Fig. 3. The NVATG over the volume of a cylindrical ^3He cell, 12 cm diameter and 10 cm long, is calculated to be $4.9 \times 10^{-4} \text{ cm}^{-1}$ for the non-identical hole compensation configuration, whereas it is $1.1 \times 10^{-3} \text{ cm}^{-1}$ for the identical hole compensation configuration. This implies an improvement in the field gradient by a factor of 2 and in the field gradient induced relaxation time by a factor of 4. Consequently, the overall gain from simulation for a MSS with a non-identical hole compensation configuration would be a factor of ≈ 16 (8 from Fig. 2 and 2 from Fig. 3) in the field gradient and ≈ 256 in the gradient-induced relaxation time over a conventional end compensation design.

IV. CONSTRUCTION AND EXPERIMENT

Magnetostatic simulation has provided good guidance for the mechanical design and construction of several MSSs. Practically, to realize the simulated gain in performance for a real MSS requires substantial care in the actual design and construction, and performance may deviate from the simulation due to imperfection in the manufacturing process for the mu-metal parts. For example, in one of our original solenoids, Gemini, there is a slight gap between the mu-metal body and the overlapping endcap section. Figure 6 shows a picture and a 3D drawing of the MSS Venus. A 90° cut is done to show the detail of the design of a MSS. A MSS includes a Co-NETIC²⁸ mu-metal cylinder, two Co-NETIC mu-metal end-caps fitted over the ends of the mu-metal cylinder with 2.5 cm overlap, an aluminum compensation coil support, and an aluminum cylinder for winding the coil on the main solenoid. On each end cap, there is a 5 mm diameter hole for access to the compensation wire. There is a notch at the edge of the end of the mu-metal cylinder and the overlap of the end cap for easy removal of the end cap during the cell exchange and access to the winding wire of the main solenoid, and both free induction decay (FID) and AFP NMR cables. The notch is 5 mm by 5 mm on the cylinder and 25 mm by 5 mm on the end cap so that the end cap can be accurately matched to the cylinder over the overlap section. The notches allow no gap between the end cap and the mu-metal cylinder. Each compensation coil support is a ring with a groove of 5.9 mm by 5.6 mm for winding and is

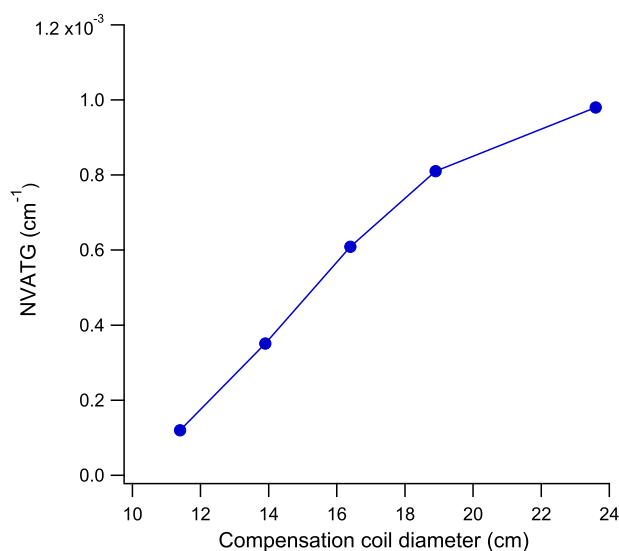


FIG. 5. The NVATG $|\vec{\nabla} B_z|/B$ as a function of the diameter of the compensation coil locations for the MSS Gemini.

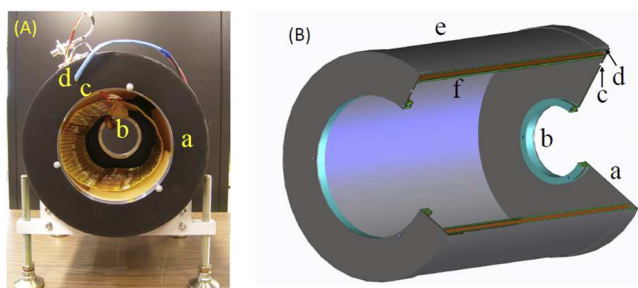


FIG. 6. (A) Picture of the MSS Venus in which an RF coil and a FID NMR coil can be seen and (B) 3D model of Venus with a 90° cut to show the detail of the compensation scheme. The MSS has the following components: (a) Co-NETIC mu-metal end cap, (b) compensation coil, (c) 3 mm diameter hole for access to the winding wire of the compensation coil, (d) 5 mm by 5 mm notch for access to the winding wire of the main coil, (e) Co-NETIC mu-metal body, and (f) the aluminum cylinder.

centered to the hole of each end cap. The gap between the compensation coil and the mu-metal end cap is 3.1 mm, which is necessary for permitting insertion of an aluminum screw. The compensation coil support is attached to the end cap using three aluminum screws with three 3 mm holes (not shown in Fig. 6) near each end cap hole. The notches and the 5 mm and 3 mm holes on the end cap were not modeled in the simulation since any perturbation to the field profile is localized (further away from the cell) and small. It is likely that a tiny gap between the overlap of the end cap and the mu-metal cylinder might exist due to the fabrication process. We estimate that the gap is typically much less than 1 mm, except for the MSS Gemini, which has a gap of 1.2 mm.

All MSSs were fabricated by Magnetic Shield Corporation.²⁸ A typical fabrication process for a MSS includes the following steps: (1) rolling a Co-NETIC mu-metal sheet to form a cylinder with the junction welded and with the small notch pre-cut at ends; (2) the Co-NETIC overlap section is rolled to an open rim shape with the opening matched to the notch, which is then welded to a circular Co-NETIC end cap cover with the hole in the center and other small holes pre-drilled to form an end cap. Simulation indicated that too sharp a turn in the mu-metal can result in field leakage; hence, a 2 mm radius of curvature was employed for the joint between the cover and the overlap section in the end cap. After welding, the roundness of the cylinder and the overlap section of the end cap and snugness between them are checked and adjusted, if necessary. The welding region is then polished and ground to produce a smooth surface. Final perfection annealing²⁸ after machining and welding was done in a controlled hydrogen atmosphere. After annealing, extra care was taken to avoid dropping or mechanical denting so as to prevent degradation of the performance when assembling and operating the MSS. We used AA perfection annealed Co-NETIC.²⁸

A single layer of 16 AWG was wound with no gap between every turn on the aluminum cylinder. Every finalized MSS is operated with a single DC power supply so that the same current is applied to both the main solenoid and compensation coils. This indicates an integer number of turns of the compensation coil. Although it is possible that the field gradient can be further slightly improved

using a partial number of turns from simulations, we decided to construct a MSS with only the integer number of turns of the compensation coil for necessity of convenient and reliable operation in a space limited neutron beam.

For experimental optimization, a computer controlled mapping system was used for measurements of the field at various compensation coil conditions. A 3-axis Hall probe [Lakeshore 460 3-channel gaussmeter with a high sensitivity (HSE) probe] and a 3-axis fluxgate magnetometer (Bartington MG-03 MS) were used to measure the field. The fluxgate magnetometer was used for measurements of fields lower than 1 mT, while the Hall probe was used for measurements of fields higher than 1 mT. The field maps with fields less than 1 mT were always checked first.

The relaxation time measurement was done using either the neutron transmission method³² on the Polarized ³He And Detector Experiment Station (PHADES) beamline at the NCNR³³ or FID NMR method.

V. RESULTS AND DISCUSSION

Over the past decade, we have designed and constructed one MSS with identical hole compensation (Gemini) and three MSSs with non-identical hole compensation (Venus, Nyx, and Honesty). Each MSS has been associated with dedicated development of one or more enhanced polarized neutron instruments. The first MSS, Gemini, was developed over 10 years ago to provide a homogeneous field for a spin analyzer for applications in small-angle neutron scattering (SANS), TAS, and reflectometry. Gemini has been often used for experiments on those instruments and sometimes for other applications such as the development of spherical neutron polarimetry on the PHADES beamline.³⁴ The MSS Venus was recently developed as a SANS analyzer with the non-identical hole compensation to increase the scattering angular (momentum transfer) coverage, improve the relaxation time, and allow for reduction of field gradients from a nearby 1.6 T electromagnet. The MSS Nyx is described in Sec. III, and the MSS Honesty was developed recently as an analyzer for the polychromatic beam reflectometer.²⁷

We have performed simulations for every MSS for optimization of the NVATG and experimentally minimized the field gradient. The experimental optimization was carried out first at low fields and then at high fields to check the consistency of the field gradients in both conditions. Field maps were taken on the axis of a MSS by varying the number of compensation turns. The NLAG along the solenoid axis was computed over a length of 10 cm centered at the most homogeneous region for each field map. A minimum NLAG is determined from a series of measurements of the field map with a varying number of compensation turns. Figure 7 shows an example of a set of normalized B_z field profiles measured in the central plane $x = 0$. Field maps on off-center axes were often taken to determine the off-axis gradients along x away from the center.

A. Field gradient determination

In Sec. II, we have discussed how to compute the field gradient induced relaxation from simulation. Here, we describe a simple approach to experimentally determine the field gradient. As described in Eq. (1), the field gradient induced relaxation T_1^{fg} can be experimentally determined by measuring the intrinsic relaxation

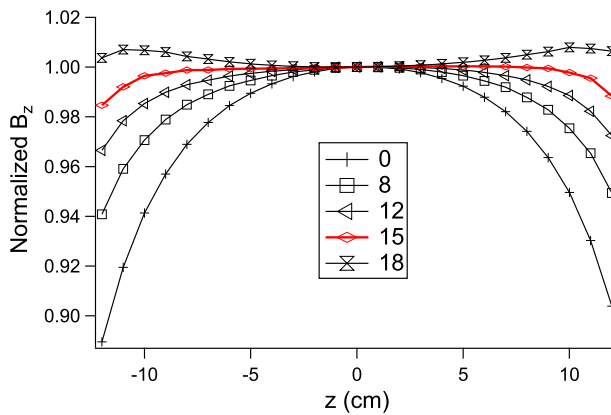


FIG. 7. Measured normalized B_z field profiles for different numbers of turns of the compensation coil during optimization of the MSS Gemini with the identical hole compensation configuration. 15 turns of compensation coil (shown in a red solid line) were determined to yield the minimum NLAG. Lines are to guide the eye. Error bars are smaller than the data points. Throughout the paper, error bars and uncertainties represent one standard deviation.

time T_1^i and the relaxation time of a ^3He cell in a MSS. T_1^i s were measured in a pair of Helmholtz coils with a diameter of 80 cm that provide a volume-averaged field gradient $\approx 10^{-4} \text{ cm}^{-1}$, corresponding to a value of T_1^{fg} of $\approx 15\,000 \text{ h}$ at a ^3He partial pressure of 1 bar. Although this approach limited determination of the field gradients in the MSSs to 10^{-4} cm^{-1} , this was sufficient for evaluation of practical NSF's and was employed for nearly all applications at the NCNR. It can be shown from Eqs. (1) and (2) that a ^3He cell with a longer T_1^i provides higher sensitivity to determination of the field gradient. Such long relaxation time cells are conveniently available from our prior cell development.¹⁴

B. Compensating the hole of the end cap

As demonstrated in Sec. II, applying fields to compensate the holes on each of the end caps significantly improves the field gradient over a conventional compensation configuration. The MSS Gemini was employed to experimentally confirm this. Gemini was first configured to have the conventional end compensation configuration, as shown in Fig. 2. After optimization through the field mapping, we characterized the performance by measuring the relaxation time of a ^3He cell in Gemini. The cell Teroldego, 11.5 cm diameter by 10 cm long with a ^3He partial pressure of 1.43 bars, was used for the measurement and had a long T_1^i of 490 h. After 3 days of decay of the ^3He polarization of Teroldego in Gemini, we obtained a relaxation time of $T_1 = (145 \pm 4) \text{ h}$ using the FID NMR method. After correcting for the intrinsic relaxation time, the NVATG $|\vec{\nabla} B_{\perp}/B|$ was determined to be $9.8 \times 10^{-4} \text{ cm}^{-1}$ in the conventional end compensation configuration. This result was obtained with seven turns of compensation. We then removed the compensation coil on the main coil and reconfigured Gemini to have the identical hole compensation configuration. After optimization of the number of turns of the compensation coil, we obtained a relaxation time of $(411 \pm 9) \text{ h}$ using the FID NMR method, which yielded a

NVATG of $2.8 \times 10^{-4} \text{ cm}^{-1}$. 15 turns of compensation were determined to be necessary at optimization in this new compensation configuration. This experimentally demonstrated that compensating the end cap hole yielded an improvement in the field gradient induced relaxation time for the cell Teroldego in the Gemini MSS by a factor of 12 compared to that obtained with the conventional end compensation configuration. This result implies an improvement in the normalized volume-averaged transverse field gradient of a factor of 3.5 in this compact MSS. The experimentally determined field gradient from the conventional end compensation configuration agreed well with that from simulation. However, the experimentally determined gradient from the identical hole compensation configuration was higher than that from simulation. This higher gradient could be due to imperfections in the real apparatus, such as the small but slightly larger air gap between the mu-metal body and the overlap of the end cap than a normal one. However, other non-ideal geometric factors such as a small difference of compensation coil location, inhomogeneous permeability in the mu-metal, roundness of the mu-metal cylinder and end caps, parallelism of the end cap, and the centering of the coil in the shield might make additional contributions to the discrepancy.

We have not configured the compensation coil in any other positions that are between the two extreme conditions as shown in Fig. 5 of Gemini and have no relaxation time data in those in-between positions. This is due to a practical consideration that there are no 3 mm holes pre-drilled for attaching the compensation coil support to an end cap. However, such configurations are not necessary since the relaxation times and the resulting gradients are expected to fall in between the two extreme conditions, that is, between 145 h and 411 h and between $9.8 \times 10^{-4} \text{ cm}^{-1}$ and $2.8 \times 10^{-4} \text{ cm}^{-1}$, respectively. Table I summarizes the result of the field gradient at two extremely different locations of the compensation coil.

The MSS was finally constructed with the identical hole compensation configuration. The finalized MSS Gemini has been used for a decade as a spin analyzer on SANS, reflectometer, and TAS beamlines. The field gradients obtained from the relaxation time from many user experiments were consistent with those obtained in this paper.

C. Compensation with non-identical coils

After demonstrating a significant improvement of the field gradient by applying the identical hole compensation, we continue to

TABLE I. Comparison of the experimentally determined NVATG $|\vec{\nabla} B_{\perp}/B|$ between the end and identical hole compensation configurations for the MSS Gemini. $\varnothing = 25.4 \text{ cm}$ and $\ell = 35.6 \text{ cm}$ are the diameter and length of the mu-metal cylinder assembly, respectively. The calculated NVATG $|\vec{\nabla} B_{\perp}/B|^{\text{cal}}$ at optimization is listed for comparison.

Compensation configuration	$ \vec{\nabla} B_{\perp}/B \text{ } 10^{-4} \text{ cm}^{-1}$	$ \vec{\nabla} B_{\perp}/B ^{\text{cal}} \text{ } 10^{-4} \text{ cm}^{-1}$
End compensation	9.8 ± 0.2	9.8
Hole compensation	2.8 ± 0.1	1.2

TABLE II. Comparison of the experimentally determined and calculated NVATG for several different MSSs with non-identical compensation coils. x and y are the required beam size along the horizontal and vertical directions at the ^3He cell position. \varnothing and ℓ are the outside diameter and length of the mu-metal assembly of the cylinder body and end caps. d_s and d_l are the diameters of the small and large holes on the end caps, respectively. T_1^e is the measured ^3He polarization relaxation time in a cavity. $|\vec{\nabla}B_{\perp}/B|$ is the NVATG determined from Eqs. (1) and (2) and the partial pressure of ^3He gas. $|\vec{\nabla}B_{\perp}/B|^{\text{cal}}$ is the calculated NVATG at optimization of a MSS. $|\vec{\nabla}B_{\perp}/B|_{\text{sym}}^{\text{cal}}$ is the calculated NVATG at optimization with larger identical compensation coils.

Solenoid	Instrument class	$x \times y$ (cm \times cm)	$\varnothing \times \ell$ (cm \times cm)	d_s (cm)	d_l (cm)	T_1^e (h)	$ \vec{\nabla}B_{\perp}/B $ (10^{-4} cm $^{-1}$)	$ \vec{\nabla}B_{\perp}/B ^{\text{cal}}$ (10^{-4} cm $^{-1}$)	$ \vec{\nabla}B_{\perp}/B _{\text{sym}}^{\text{cal}}$ (10^{-4} cm $^{-1}$)
Honesty	Reflectometer	12×4	27.9×35.6	11.7	14.3	415 ± 3	3.7 ± 0.2^{27}	3.5	4.8
Nyx	TAS	5×10	25.5×29.5	10.3	12.6	370 ± 8	4.2 ± 0.2	4.9	11.0
Venus	SANS	12×12	25.4×33.0	9.0	16.0	300 ± 10	4.4 ± 0.2	5.6	11.0

show that a further improvement can be experimentally achieved by applying non-identical hole compensation. To show the effect, we present the results from three MSSs that were required for three different polarized beam instruments, SANS, TAS, and reflectometer at the NCNR. These applications represent many conventional but powerful polarized neutron instruments for studies of magnetism. Different ^3He cells with intrinsic relaxation times longer than 450 h were used to experimentally determine the NVATG. These cylindrical cells have dimensions about 12 cm diameter and 10 cm length. The results are summarized in Table II. Also listed in Table II are the calculated values of $|\vec{\nabla}B_{\perp}/B|$ for the configurations of non-identical hole compensation and identical hole compensation with the larger endcap hole. For SANS, a circular beam size of 12 cm in diameter is chosen, which represented the largest angular coverage we could have accomplished. The calculated gradients with the non-identical compensation configuration are up to a factor of 2.2 smaller than that with identical larger compensation coils. This implied an additional improvement in the gradient induced relaxation time by

a factor of more than 4. (Of course, no improvement would be obtained from this approach for a collimated beam.) We note that only an integer number of turns of compensation coils were used for simulation. A partial number of turns of compensation coils may further improve the field gradient. We speculate that this may be a reason why the experimentally determined NVATG is better than that from simulation. In addition, the more complicated procedure described in Sec. III to optimize the non-identical hole compensation configuration may have not yielded the conditions for the actual optimum.

D. Size of the homogeneous magnetic field region

A fundamental yet essential goal in designing a magnetostatic cavity for a NSF application is to have the volume of the homogeneous region as large as possible while still fitting the cavity into a constrained space. In many cases, an existing magnetostatic cavity uses a significant amount of space and/or its NVATG is not

TABLE III. Comparison of the ratio Υ of the volume of the homogeneous field region to that of the device itself from various designs of the magnetostatic cavities. The dimensions are diameter \varnothing and length l for the mu-metal assembly of the cylinder body and end caps for a MSS, and width w , height h , and length l for a magic box. d_h and l_h are the diameter and length of the cylinder of the homogeneous field region. The data of the magnetostatic cavity devices of the last six rows are from other labs.

Cavity name	Cavity type	Dimensions (cm \times cm)	Υ	Instrumentclass	P or A	$d_h \times l_h$ (cm \times cm)	$ \vec{\nabla}B_{\perp}/B $ (10^{-4} cm $^{-1}$)
Gemini	Solenoid	25.4×35.6	0.064	TAS/SANS ²⁶	Analyzer	12×10	2.8 ± 0.1
Kronos	Solenoid	20.3×25.4	0.14	TAS/SANS ²⁵	Polarizer	12×10	6.0
Venus	Solenoid	25.4×33	0.061	SANS	Analyzer	12×9	4.4 ± 0.2
Honesty	Solenoid	27.9×35.6	0.055	Reflectometer ²⁷	Analyzer	13×9	3.7 ± 0.2
Nyx	Solenoid	25.1×29.2	0.078	TAS	Polarizer	12×10	4.2 ± 0.2
Flattop	Magic box	$40 \times 15 \times 28.4$	0.066	TAS ¹⁷	Polarizer	12×10	5.7 ± 0.4
	Solenoid ²⁴	27.2×36.4	0.037		Polarizer	10×10	<4.0
	Solenoid	30×46	0.024	TAS ²¹	Analyzer	10×10	2.0
	Solenoid	9.5×20	0.030	SCD ¹⁰	Polarizer	3×6	45.0
	Solenoid	20×30	0.030	POLANO ²³	Polarizer	6×10	<10.0
	Magic box	$20 \times 40 \times 78$	0.015	TOPAS ³⁵	Polarizer	12×8	4.4
	Magic box	$30 \times 40 \times 62$	0.012	MARIA ³⁵	Analyzer	12×8	<2.0
	Magic box ¹⁸	$40 \times 17 \times 80$	0.005			6×10	<2.0
	Solenoid ¹⁹	33×96	0.003			8×8	<1.0

minimized. Here, we present a benchmark to accomplish this goal and show that an optimized compensation scheme can achieve a larger region of field homogeneity for a MSS. Define Y to be the ratio of the volume of the most homogeneous field region in which the cell is located to that occupied by the magnetostatic cavity. The larger this ratio, the more compact the magnetostatic cavity.³⁶ Table III summarizes a comparison of the value of Y from various designs of the magnetostatic cavities for a wide variety of NSF applications on a great variety of polarized neutron instruments at various neutron facilities. We present the ratios Y not only for the developed MSSs in this work but also for magic boxes operated as either a polarizer or analyzer.^{2,10,23,25,26,35} It can be seen that MSSs typically provide larger values of Y than magic boxes with the exception of end-compensated magic boxes.¹⁷ For offline operation in which ^3He gas is polarized off the beamline, it is apparent that a MSS is advantageous over a magic box in implementation of a NSF in a constrained space and is generally better at shielding stray fields. When comparisons are made among the different MSSs, we show that placing compensation coils centered around the hole of the end cap provides significant advantage in minimizing the field gradient or saving space or rendering a larger angular coverage. Implementing non-identical hole compensation coils centered around the non-identical holes of the end caps resulted in an overall improvement in the field gradient induced relaxation of the ^3He polarization by a factor of ≈ 50 compared to a conventional end compensation design of a MSS and brought the operation of several polarized neutron instruments at the NCNR to a new stage with much better performance, greater reliability, and more reduced maintenance. The new approach would make the existing MSS-based *in situ* SEOP systems, for example, Refs. 22 and 23, more compact without degrading the relaxation time, hence the performance.

VI. CONCLUSIONS

We have simulated and optimized the magnetic field gradients of several magnetically shielded solenoids (MSSs) for ^3He storage of neutron spin filters that have been employed at several conventional, nevertheless, powerful polarized neutron instruments at the NCNR. The conveniently measurable line-averaged field gradient along the solenoid center axis has been confirmed in simulation as a good indicator for the transverse field gradients that are directly related to the field gradient-induced ^3He polarization relaxation time in MSSs. Magnetic field simulations have provided solid guidance in designing a MSS. We have constructed and characterized several MSSs and find that placing the compensation coils centered around the hole of the end caps of a MSS has yielded an improvement in the volume-averaged transverse gradient by a factor of 3.5. For a MSS of 25 cm diameter and 35.6 cm length, this corresponds to an improvement of a factor of 12 in the gradient induced relaxation time over that with a conventional configuration in which the compensation coils are placed on the main coil. A further improvement in the gradient up to a factor of 2 has been confirmed by implementing a non-identical compensation coil centered around the non-identical hole in the end cap. Consequently, all MSSs constructed using the new compensation coil configuration show a volume-averaged transverse gradient better than $5 \times 10^{-4} \text{ cm}^{-1}$ for a volume of $\approx 1000 \text{ cm}^3$ in a compact space. We have shown that these newly developed MSSs yield

a significantly larger ratio of the field homogeneity volume to that of the device itself. The enhanced approach has resulted in significant improvement in the ^3He polarization relaxation time and/or allowed more compact designs for ^3He NSFs for a wide variety of polarized neutron instruments at the NCNR. The improvement has greatly facilitated the routine polarized beam experiments on the instruments including the SANS instrument, thermal TAS, and the reflectometer. The enhanced design of magnetostatic cavities can be applied to other neutron scattering facilities and other scientific applications demanding a high level of field homogeneity with a large volume.

ACKNOWLEDGMENTS

The authors thank Jeff Anderson and Aaron Kirchhoff of the NIST Optical Shop for their assistance with fabrication of cells. The work utilized facilities supported, in part, by the National Science Foundation under Agreement No. DMR-1508249.

DATA AVAILABILITY

The data that support the findings of this study are available within the article.

REFERENCES

- ¹K. H. Andersen, R. Chung, V. Guillard, H. Humblot, D. Jullien, E. Lelièvre-Berna, A. Petoukhov, and F. Tasset, *Physica B* **356**, 103 (2005).
- ²W. C. Chen, T. R. Gentile, R. Erwin, S. Watson, Q. Ye, K. L. Krycka, and B. B. Maranville, *J. Phys.: Conf. Ser.* **528**, 012014 (2014).
- ³E. Babcock and A. Ioffe, *J. Phys.: Conf. Ser.* **294**, 012005 (2011).
- ⁴H. Kira, Y. Sakaguchi, T. Oku, J. Suzuki, M. Nakamura, M. Arai, Y. Endoh, L. J. Chang, K. Kakurai, Y. Arimoto, T. Ino, H. M. Shimizu, T. Kamiyama, K. Ohoyama, H. Hiraka, K. Tsutsumi, and K. Yamada, *J. Phys.: Conf. Ser.* **294**, 012014 (2011).
- ⁵C. Y. Jiang, X. Tong, D. R. Brown, W. T. Lee, H. Ambaye, J. W. Craig, L. Crow, H. Culbertson, R. Goyette, M. K. Graves-Brook, M. E. Hagen, B. Kadron, V. Lauter, L. W. McCollum, J. L. Robertson, B. Winn, and A. E. Vandegrift, *Phys. Procedia* **42**, 191 (2013).
- ⁶P. A. M. Dolph, J. Singh, T. Averett, A. Kelleher, K. E. Mooney, V. Nelyubin, W. A. Tobias, B. Wojtkowski, and G. D. Cates, *Phys. Rev. C* **84**, 065201 (2011).
- ⁷Q. Ye, G. Laskaris, W. Chen, H. Gao, W. Zheng, X. Zong, T. Averett, G. D. Cates, and W. A. Tobias, *Eur. Phys. J. A* **44**, 55 (2010).
- ⁸M. S. Albert *et al.*, *Nature* **370**, 199 (1994); E. J. R. van Beek *et al.*, *J. Magn. Reson. Imaging* **20**, 540 (2004).
- ⁹T. R. Gentile, P. J. Nacher, B. Saam, and T. G. Walker, *Rev. Mod. Phys.* **89**, 045004 (2017).
- ¹⁰G. L. Jones, J. Baker, W. C. Chen, B. Collett, J. A. Cowan, M. F. Dias, T. R. Gentile, C. Hoffmann, T. Koetzle, W. T. Lee, K. Littrell, M. Miller, A. Schultz, W. M. Snow, X. Tong, H. Yan, and A. Yue, *Physica B* **356**, 86–90 (2005).
- ¹¹N. R. Newbury, A. S. Barton, G. D. Cates, W. Happer, and H. Middleton, *Phys. Rev. A* **48**, 4411 (1993).
- ¹²W. A. Fitzsimmons, L. L. Tankersley, and G. K. Walters, *Phys. Rev.* **179**, 156 (1968).
- ¹³L. D. Schearer and G. K. Walters, *Phys. Rev.* **139**, A1398–A1402 (1965).
- ¹⁴W. C. Chen, T. R. Gentile, C. B. Fu, S. Watson, G. L. Jones, J. W. McIver, and D. R. Rich, *J. Phys.: Conf. Ser.* **294**, 012003 (2011), and references therein.
- ¹⁵Z. Salhi, E. Babcock, P. Pistel, and A. Ioffe, *J. Phys.: Conf. Ser.* **528**, 012015 (2014).
- ¹⁶G. D. Cates, S. R. Schaefer, and W. Happer, *Phys. Rev. A* **37**, 2877 (1988).

- ¹⁷J. W. McIver, R. Erwin, W. C. Chen, and T. R. Gentile, *Rev. Sci. Instrum.* **80**, 063905 (2009).
- ¹⁸A. K. Petoukhov, V. Guillard, K. H. Andersen, E. Bourgeat-Lami, R. Chung, H. Humblot, D. Jullien, E. Lelievre-Berna, T. Soldner, F. Tasset, and M. Thomas, *Nucl. Instrum. Methods Phys. Res., Sect. A* **560**, 480 (2006).
- ¹⁹R. J. Hanson and F. M. Pipkin, *Rev. Sci. Instrum.* **36**, 179 (1965).
- ²⁰W. Heil, J. Dreyer, D. Hofmann, H. Humblot, E. Lelievre-Berna, and F. Tasset, *Physica B* **267–268**, 328–335 (1999).
- ²¹T. R. Gentile, E. Babcock, J. A. Borchers, W. C. Chen, D. Hussey, G. L. Jones, W. T. Lee, C. F. Majkrzak, K. V. O'Donovan, W. M. Snow, X. Tong, S. G. E. te Velthuis, T. G. Walker, and H. Yan, *Physica B* **356**, 96–102 (2005).
- ²²X. Tong, C. Y. Jiang, V. Lauter, H. Ambaye, D. Brown, L. Crow, T. R. Gentile, R. Goyette, W. T. Lee, A. Parizzi, and J. L. Robertson, *Rev. Sci. Instrum.* **83**, 075101 (2012).
- ²³T. Ino, M. Ohkawara, K. Ohoyama, T. Yokoo, S. Itoh, Y. Nambu, M. Fujita, H. Kira, H. Hayashida, K. Hiroi, K. Sakai, T. Oku, and K. Kakurai, *J. Phys.: Conf. Ser.* **862**, 012011 (2017).
- ²⁴H. Kira, Y. Sakaguchi, J. Suzuki, T. Oku, M. Nakamura, M. Arai, K. Kakurai, Y. Endo, Y. Arimoto, T. Ino, H. M. Shimizu, T. Kamiyama, K. Ohoyama, H. Hiraka, K. Tsutsumi, K. Yamada, and L.-J. Chang, *Phys. Procedia* **42**, 200–205 (2013).
- ²⁵W. C. Chen, G. Armstrong, Y. Chen, B. Collett, R. Erwin, T. R. Gentile, G. L. Jones, J. W. Lynn, S. McKenney, and J. E. Steinberg, *Physica B* **397**, 168–171 (2007).
- ²⁶W. C. Chen, R. Erwin, J. W. McIver III, S. Watson, C. B. Fu, T. R. Gentile, J. A. Borchers, J. W. Lynn, and G. L. Jones, *Physica B* **404**, 2663–2666 (2009).
- ²⁷M. T. Hassan and W. C. Chen, *J. Phys.: Conf. Ser.* **1316**, 012017 (2019).
- ²⁸Magnetic Shield Corporation, 740 N. Thomas Drive, Bensenville IL 60106. Either perfection annealing or perfection annealed is the terminology for the annealing process from the company. Certain trade names and company products are mentioned in the text or identified in an illustration in order to adequately specify the experimental procedure and equipment used. In no case does such identification imply recommendation or endorsement by the National Institute of Standards and Technology, nor does it imply that the products are necessarily the best available for the purpose.
- ²⁹O. Chubar, P. Elleaume, and J. Chavanne, *J. Synchrotron Radiat.* **5**, 481 (1998).
- ³⁰See <http://www.wolfram.com/mathematica/> for information about Wolfram Mathematica.
- ³¹We note that names for the magnetically shielded solenoids and ^3He cells are used throughout the paper. Such names were used in our previous papers.^{2,14}
- ³²G. L. Jones, T. R. Gentile, A. K. Thompson, Z. Chowdhuri, M. S. Dewey, W. M. Snow, and F. E. Wietfeldt, *Nucl. Instrum. Methods Phys. Res., Sect. A* **440**, 772–776 (2000).
- ³³See <https://ncnr.nist.gov/instruments/instdev.html> for information about the PHADES beam line.
- ³⁴J. Tosado, W. C. Chen, S. Gnewuch, T. Hasaan, T. Dax, and E. E. Rodriguez, *Rev. Sci. Instrum.* **90**, 063303 (2019).
- ³⁵E. Babcock, Z. Salhi, L. Barnsley, J. Voigt, S. Mattauch, and A. Ioffe, *J. Phys.: Conf. Ser.* **1316**, 012019 (2019).
- ³⁶We note that the compactness of the device is particularly important for ^3He NSF applications at the NCNR but may not be the only consideration to be taken at other institutions or facilities.